Applied Mathematical Modelling 37 (2013) 1860–1871

Contents lists available at SciVerse ScienceDirect

Applied Mathematical Modelling

journal homepage: www.elsevier.com/locate/apm

Lattice Boltzmann equation model for multi-component multi-phase flow with high density ratios

Jie Bao [a], Laura Schaefer [b,*]

[a] Fluid and Computational Engineering Group, Pacific Northwest National Laboratory, WA 99352, USA
[b] Department of Mechanical Engineering and Materials Science, University of Pittsburgh, Pittsburgh, PA 15261, USA

ARTICLE INFO

Article history:
Received 22 June 2010
Received in revised form 23 April 2012
Accepted 27 April 2012
Available online 9 May 2012

Keywords:
Lattice Boltzmann equation (LBE) model
Multi-component multi-phase (MCMP)
High density ratio

ABSTRACT

Multi-component multi-phase (MCMP) flows are very common in engineering or industrial problems, as well as in nature. Because the lattice Boltzmann equation (LBE) model is based on microscopic models and mesoscopic kinetic equations, it offers many advantages for the study of multi-component or multi-phase flow problems. While the original formulation of Shan and Chen's (SC) model can incorporate some MCMP flow scenarios, the density ratio of the different components is greatly restricted to less than approximately 2.0. This obviously limits the applications of this MCMP LBE model. Hence, based on the original SC MCMP model and the improvements in the single-component multi-phase (SCMP) flow model reported by Yuan and Schaefer, we have developed a new model that can simulate a MCMP system with a high density ratio.

1. Introduction

Multi-component multi-phase (MCMP) flow can be generally divided into three categories: liquid–gas, solid–gas and solid–liquid systems. This paper focuses on liquid–gas flow interactions. Liquid–gas systems are very common in engineering and industrial problems, such as in boilers, condensers and nuclear reactors, or in nature, like rain and fog. The importance of MCMP flow has led to the development of many methods and models to study it. There are several approaches to simulating multiphase flows based on traditional CFD methods. The main function of multiphase models is tracking the free surface between different phases/components, the means for which can be divided into two categories: the front-capturing method and the front-tracking method. Front-capturing methods track the movement of the fluid and "capture" the interface afterwards. In these methods, the two phases are modeled as a single continuum with discontinuous properties at the interface. The most widely used front capturing methods are the Marker-and Cell (MAC) method [1,2], Volume-of-Fluid (VOF) method [3], and level set method [4]. Front-tracking methods directly "track" the location of the two-phase interface, so they allow more accurate calculation of the curvature of the free surface [5]. The most commonly used front-tracking methods are the boundary-fitted grid method [6], Tryggvassion's hybrid method [7], and the Boundary Element Method (BEM) [8]. Although conceptually simple, tracking/capturing the free surface and generating a dynamic mesh are always computationally challenging tasks, especially for rapidly transient, high density ratio cases, and complicated solid boundary problems.

The phase segregation and surface tension in multiphase flow are due to the interparticle forces/microscopic interactions, and the lattice Boltzmann equation (LBE) method is capable of incorporating these interactions without tracking/capturing the interface between immiscible phases/components (which is difficult to implement in traditional CFD methods). Hence,

* Corresponding author. Address: Department of Mechanical Engineering and Materials Science, University of Pittsburgh, 153 Benedum Hall, 3700 O'Hara St., Pittsburgh, PA 15261, USA. Tel.: +1 412 624 9793; fax: +1 412 624 4846.
E-mail address: las149@pitt.edu (L. Schaefer).

0307-904X/$ - see front matter © 2012 Elsevier Inc. All rights reserved.
http://dx.doi.org/10.1016/j.apm.2012.04.048

the LBE method has attracted much recent attention in simulating multiphase flow. The LBE model has been used for many kinds of simulations of incompressible viscous flows [9]. As a relatively new numerical scheme, the LBE model has recently achieved considerable success in simulating fluid flows and associated transport phenomena. The true strengths of the LBE model lie in its ability to simulate multi-phase flows for both single and multi-component fluids [10,11].

There have been a number of LBE multiphase flow models presented in the literature. The first immiscible multiphase LBE model, proposed by Gunstensen et al. [12], used red- and blue- colored particles to represent two kinds of fluids. The phase separation is then produced by the repulsive interaction based on the color gradient and color momentum. Their model was based on the Rothman–Keller (RK) model of immiscible cellular-automaton fluids [13]. A different model proposed by Shan and Chen (SC) imposes a non-local interaction between fluid particles at neighboring lattice sites [14–17]. The interaction potentials control the form of the equation of state (EOS) of the fluid. Phase separation occurs automatically when the interaction potentials are properly chosen. In comparing the two models, Hou et al. [18] found that the SC model produced more stable and accurate results, since the magnitude of the spurious currents at the interface was less for the SC model. However, more recent work [19] has suggested that the spurious currents in the RK model can be reduced when the Latva–Kokko recoloring operator [20] is adapted to the Reis and Phillips RK model [21].

There is also the so-called free-energy-based approach proposed by Swift et al. [22,23]. In this model, the description of non-equilibrium dynamics, such as Cahn–Hilliard's approach, is incorporated into the LBE model by using the concepts of the free energy function. The free energy model has a sound physical basis, and, unlike the SC model, the local momentum conservation is satisfied. However, this model does not satisfy Galilean invariance and some unphysical effects will be produced in the simulation [24]. In the multiphase model proposed by He, Chen and Zhang (HCZ), two sets of PDFs are employed [25,26]. The first PDF set is used to simulate pressure and velocity fields and another PDF set is used to capture the interface only, which makes this approach essentially close to the interface capturing methods in spirit. Their approach is more flexible in implementing the thermodynamics of the flow. A severe problem with their approach is its numerical instability.

It should be noted that there are some cases where a two-component system does not necessarily need a two-component numerical model, such as a water–air system. Although the water and the air are two components with completely different chemical compositions, the system can be simulated by a high density ratio single-component multi-phase numerical model as demonstrated in Refs. [27–30]. However, for some cases, a real multi-component model may be needed, such as the simulation and investigation of humidity changes in a gaseous environment. We will discuss these cases in the following sections. Moreover, when heat transfer is considered, it is easier to apply different thermal properties, such as heat capacity and conductivity, to the different components if a real multi-component numerical model is used.

In practical problems, the density ratio $\left(\frac{\rho_{\text{Component1}}}{\rho_{\text{Component2}}}\right)$ of the different components can vary across a large range for different cases. For example, the density ratio of a liquid alloy system is around 1.0, while the density ratio of a water–air system maybe around 1000. The original LBE model proposed by Shan and Chen (SC) [14–17], which is the most commonly used LBE model, can only simulate a system whose density ratio is smaller than 2.0. More recent research also failed to greatly increase the density ratio of between components [31], which is still smaller than 2.0. For larger density ratios, the simulation fails due to the generation of either an infinite or negative density.

In this paper, we introduce a MCMP LBE model that can simulate problems with density ratios approaching 1000:1. In addition to greatly increasing the maximum density ratio for simulation of MCMP flows, this model also demonstrates a better velocity distribution for SCMP flows.

2. Development of the multi-component multi-phase lattice Boltzmann equation model

2.1. Equation development

The LBE model is derived from the continuum Boltzmann-BGK equation, which is a simplified form of the original continuum Boltzmann equation [32]. For MCMP flow, the evolution equation, after being discretized in momentum, physical, and time space can be written as [33]:

$$f_{\alpha,i}(\vec{x}+\vec{e}_\alpha\Delta t, t+\Delta t) = f_{\alpha,i}(\vec{x},t) - \frac{1}{\tau_i}[f_{\alpha,i}(\vec{x},t) - f^{\text{eq}}_{\alpha,i}(\vec{x},t)]\,\alpha = 0,1,\ldots N, \tag{1}$$

where f_α is the particle distribution function (PDF) along the αth-direction and f^{eq} is its corresponding equilibrium PDF [34], Δt is the time step, $\vec{e}_\alpha$ is the particle velocity in the αth-direction, τ is the non-dimensional relaxation time, and i refers to the component.

The local mass density ρ and the local velocity in the lattice unit for each component are obtained from:

$$\rho_i = \sum_{\alpha=0}^{N} f_{\alpha,i}, \tag{2}$$

$$\vec{u}_i = \frac{1}{\rho}\sum_{\alpha=0}^{N} f_{\alpha,i}\vec{e}_\alpha. \tag{3}$$

Because there is more than one component, a composite macroscopic velocity $\vec{u}'$ is needed to represent the flow of the bulk fluid:

$$\vec{u}' = \frac{\sum_i \frac{1}{\tau_i} \sum_{\alpha=0}^{N} f_{\alpha,i} \vec{e}_\alpha}{\sum_i \frac{1}{\tau_i} \sum_{\alpha=0}^{N} f_{\alpha,i}}. \tag{4}$$

The viscosity is defined in the LBE model as:

$$\upsilon = \left(\tau - \frac{1}{2}\right) c_s^2 \Delta t, \tag{5}$$

where c_s is the speed of sound in the LBE model and is equal to $\frac{\Delta x}{\Delta t\sqrt{3}}$. Hence, the viscosity can be changed by choosing a different relaxation time τ for different components.

In a LBE simulation, a D2Q9 state space, with nine velocity directions on a 2-D square lattice, is widely used for 2-D problems [35]. For 3-D flow, there are several cubic lattice models, such as the D3Q15, D3Q19, and D3Q27 model. Based on these frame definitions, the equilibrium PDF $f_{\alpha,i}^{\mathrm{eq}}$ can be expressed in the form of a quadratic expansion of the Maxwellian distribution [32]:

$$f_{\alpha,i}^{\mathrm{eq}} = \rho_i w_\alpha \left[1 + \frac{3}{c^2} \vec{e}_\alpha \cdot \vec{u}_i + \frac{9}{2c^4} (\vec{e}_\alpha \cdot \vec{u}_i)^2 - \frac{3}{2c^2} \vec{u}_i \cdot \vec{u}_i\right] \tag{6}$$

where w_α is the weighting factor, $c = \frac{\Delta x}{\Delta t}$ is the lattice speed, and Δx is the lattice constant. The weighting factors and discrete velocities for the D2Q9 model (which was used in this work) are, for example:

$$\vec{e}_\alpha = \begin{cases} (0,0), & \alpha = 0; \\ (\pm 1, 0)c, (0, \pm 1)c, & \alpha = 1,2,3,4; \\ (\pm 1, \pm 1)c, & \alpha = 5,6,7,8, \end{cases} \tag{7a}$$

$$w_\alpha = \begin{cases} 4/9, & \alpha = 0; \\ 1/9, & \alpha = 1,2,3,4; \\ 1/36, & \alpha = 5,6,7,8. \end{cases} \tag{7b}$$

It is commonly accepted that the separation of different phases or components is microscopically due to the long-range interaction between the molecules of the fluid [16]. This interaction force includes two parts for the multi-component fluid. One is the interaction between molecules from the same component, and another is the interaction between molecules from different components. These two parts can be expressed in a similar form, and are given as:

$$\vec{F}_{i,i}(\vec{x}) \cong -c_0 \psi_i(\vec{x}) g_{ii} \nabla \psi_i(\vec{x}), \tag{8a}$$

$$\vec{F}_{i,j}(\vec{x}) \cong -c_0 \psi_i(\vec{x}) g_{ij} \nabla \psi_j(\vec{x}) \quad i \neq j, \tag{8b}$$

where c_0 is a constant that depends on the lattice structure. For the D2Q9 and D3Q19 lattices, $c_0 = 6.0$, and for the D3Q15 lattice, $c_0 = 10.0$. The coefficient for the strength of the interparticle force is g, with $g < 0$ representing an attractive force between particles and $g > 0$ a repulsive force. $\vec{F}_{i,j}$ is the force between the different particles of component i, and $\vec{F}_{i,j}$ indicates the force between the component i and component j, $\psi(\vec{x})$ is the effective mass, which is a function of local density and can be varied to reflect different equations of state (EOS).

These two equations are derived from the original SC model. Although that work only used the interparticle forces of nearest neighbor sites, it can be extended to include other neighboring sites as long as the gradient term $\nabla\psi$ is properly specified. We use both the nearest and next-nearest sites to evaluate this gradient term, which gives a six-point scheme for two dimensions:

$$\frac{\partial \psi(i,j)}{\partial x} = c_1[\psi(i+1,j) - \psi(i-1,j)] + c_2[\psi(i+1,j+1) - \psi(i-1,j+1) + \psi(i+1,j-1) - \psi(i-1,j-1)], \tag{9a}$$

$$\frac{\partial \psi(i,j)}{\partial y} = c_1[\psi(i,j+1) - \psi(i,j-1)] + c_2[\psi(i+1,j+1) - \psi(i+1,j-1) + \psi(i-1,j-1) - \psi(i-1,j-1)], \tag{9b}$$

where c_1 and c_2 are the weighting coefficients for the nearest and next nearest sites, respectively. The next-nearest sites can reduce the anisotropy of the discretized momentum space, which can aid in reducing the spurious currents in the multiphase LBE model.

In addition to the interparticle forces, if the problem includes an interface of different fluid components contacting a solid surface, such as a liquid droplet on a solid surface, the interaction between the fluid and solid interface needs to be considered for adjusting the contact angle [36]. Hence, in addition to the bounce back boundary condition for streaming the

distribution function near the solid wall boundary, an extra interparticle force is added onto the particle that contacts the solid surface to correctly represent the behavior of the contact angle:

$$\vec{F}_{w,i}(\vec{x}) = -\rho_i(\vec{x})\sum_{\vec{x}'} G_{w,i}(\vec{x},\vec{x}')\rho_w(\vec{x}')(\vec{x}'-\vec{x}), \tag{10}$$

where $G_{w,j}(\vec{x},\vec{x}')$ reflects the intensity of the fluid–solid interaction, and $\rho_w(\vec{x}')$ is the wall density, which equals one at the wall and zero in the fluid. If there is no liquid–gas interface contacting a solid surface, which means that there is no significant fluid density change near a solid boundary, Eq. (10) is not necessary. Finally, the body force can be defined as:

$$\vec{F}_{b,i}(\vec{x}) = \rho_i(\vec{x})\vec{a}. \tag{11}$$

2.2. MCMP flow specifications

The density ratio is only one defining characteristic of a MCMP flow system. For example, a water–air system and an oil–air system perform very differently, although they have a similar density ratio. To capture these effects, the viscosity and the surface tension are two important factors. For freely adjusting surface tension, an additional force term should be introduced to the fluid–fluid interaction, and it is defined as:

$$\vec{F}_s = \kappa\psi(\rho)\nabla\nabla^2\psi(\rho), \tag{12}$$

where κ determines the strength of the surface tension [37].

Hence, the total force on each particle can be expressed as:

$$\vec{F}_{\text{total},i} = \vec{F}_{i,i} + \vec{F}_{i,j} + \vec{F}_{w,i} + \vec{F}_{b,i} + \vec{F}_{s,i}\cdots \tag{13}$$

All of these forces can be incorporated into the model by shifting the velocity in the equilibrium distribution. This means that the velocity $\vec{u}$ in Eq. (3) is replaced by

$$\vec{u}_i^{\text{eq}} = \vec{u}_i + \frac{\tau_i\vec{F}_{\text{total},i}}{\rho_i(\vec{x})}. \tag{14}$$

To increase the density ratio between different components, one first should increase the density ratio for the different phases of each single component. A good deal of work has already been devoted to increasing the density ratio for single-component multi-phase (SCMP) flows. For example, as reported by Swift(23), the maximum density ratio obtained using the free-energy-based approach is less than 10:1, and the largest density ratio tested in the He, Chen and Zhang (HCZ) approach is 40:1 [38]. These are improvements, but are still not large enough for most practical problems. This is because the ideal gas EOS and original SC model show unrealistic pressure-density relationships. They give a high compressibility for the liquid phase, which is even higher than the vapor phase. Yuan and Schaefer [39] found, however, that is possible to simulate SCMP flows with a density ratio that can easily reach 1000:1 by using a more accurate EOS, such as the van der Waals, Peng–Robinson, or Carnahan-Starling EOS [40]. A density ratio of this magnitude means that the LBE model is suitable for simulation of most single-component vapor-liquid flows.

The effective mass is the mechanism for incorporating a more sophisticated EOS. As stated previously, the effective mass $\psi(\vec{x}) = \psi(\rho(\vec{x}))$ is a function of the local density, and can be defined as:

$$\psi_i(\rho) = \sqrt{\frac{2(p_i - c_s^2\rho_i)}{c_0 g_{ii}}}, \tag{15}$$

where p is the pressure. The choice of EOS can reflect the relationship between the pressure, temperature and density. In Yuan and Schaefer [39], five different EOS were tested in this model, and it was found that that the Peng–Robinson (P–R) EOS provided a maximum increase in the density ratio of SCMP flows while maintaining small spurious currents around the interface. (The other equations of state also provided improvements over the SC EOS, but did not reduce the spurious current as significantly; a more detailed comparison is given in [39].) Hence, we will use the P–R EOS in this MCMP flow research, where the P–R EOS is expressed as:

$$P = \frac{\rho RT}{1-b\rho} - \frac{a\alpha(T)\rho^2}{1+2b\rho-b^2\rho^2}, \tag{16}$$

$$\alpha(T) = [1 + (0.37464 + 1.5422\omega - 0.26992\omega^2)(1-\sqrt{T/T_c})]^2. \tag{17}$$

with $a = \frac{0.45724R^2T_c^2}{P_c}$, $b = \frac{0.0778RT_c}{P_c}$, where a is the attraction parameter, $b$is the repulsion parameter, R is the gas constant, ω is the acentric factor, and T_c and P_c are the critical temperature and critical pressure, respectively. T is the temperature, and can be used to control the density ratio. When T is smaller than the critical temperature, phase separation occurs, and a smaller temperature leads to a larger density ratio. In this study, only isothermal systems are considered, so T is constant. However, when evaluating a system with thermal effects, an actual temperature field can be applied to Eq. (16) and (17). For a given

fluid and temperature field, α, a, and b can be found, so that Eq. (16) is solely a function of pressure, density, and the temperature field. Eq. (16) is then substituted in for the pressure term in Eq. (15), and the effective mass ψ_i can be calculated from a known density and temperature field.

Unlike in the original SC model, the coefficient of interaction strength within a component (g_{ii}) here cannot control the overall interaction strength. (Indeed, it is canceled out when we substitute Eq. (15) into Eq. (8a)). The only requirement for g_{ii} is to ensure that the whole term inside the square root is positive. However, we have found that the coefficient of interaction strength between different components g_{ij} is very important for creating and extending the MCMP LBE model. Firstly, when Eq. (15) is substituted into Eq. (8b), g_{ij} will not be canceled. Secondly, from Eq. (8b), it can be seen that g_{ij} affects the magnitude of the interparticle force between different components $F_{i,j}$. The behavior of interactions between different components is mainly controlled by this force, so the interaction can be adjusted through changing the value of g_{ij}. From our tests, this force plays a critical role in adjusting the system density ratio, which we will explain and demonstrate in the following section.

3. Simulation results

3.1. Simulation of an equilibrium droplet without body forces and external forces

The first example is the simulation of a circular droplet in a 100 × 100lattice 2D square domain for a liquid–gas system without body forces. A periodical boundary condition is applied on the four boundaries. Fig. 1(a) shows the density distribution of both components and Fig. 2(a) shows the comparison of the density of the two components along the centerline ($y = 50$, $0 \leqslant x \leqslant 100$) on a $\log_{10}$ scale. For convenience, we have highlighted several segments on these lines, which are the maximum density of component 1, minimum density of component 1, maximum density of component 2, and minimum density of component 2, noted as $\rho_{\text{Component1,max}}$, $\rho_{\text{Component1,min}}$, $\rho_{\text{Component2,max}}$, and $\rho_{\text{Component2,min}}$, respectively. The density variation in each segment is very small compared to the density change at the interface of the different components, so this small variation can be neglected. In Fig. 2(a), the density of component 1in the droplet ($\rho_{\text{Component1,max}}$) is on the order of 10^1, while the density of component 2 around the droplet ($\rho_{\text{Component2,max}}$) is on the order of 10^{-2}. Hence the density ratio of these two components is around 1000:1. In general, the density ratio of a system refers to the ratio between the maximum densities of the two components ($\frac{\rho_{\text{Component1,max}}}{\rho_{\text{Component2,max}}}$). Our model is also can be used for a system that contains more than 2 components, Fig. 1(b) shows a 3-component system, and Fig. 2(b) shows the comparison of the density of the three components along the center line.

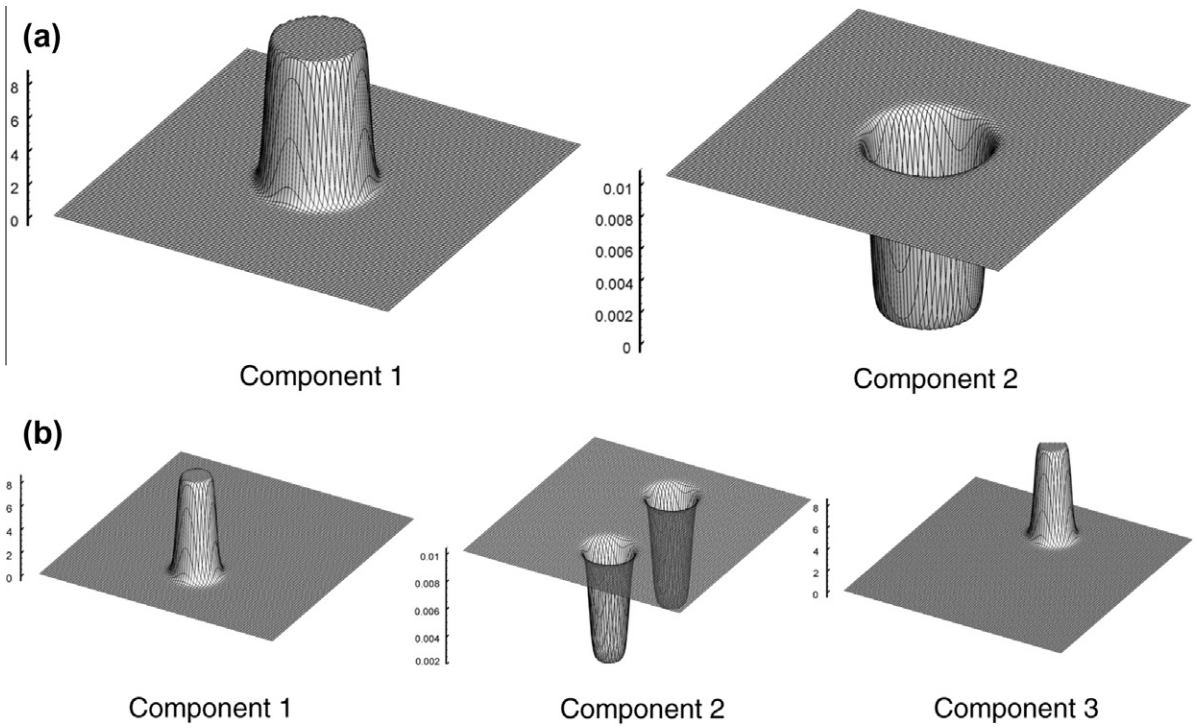

Fig. 1. (a) Density distribution of each component for a two-component system, (b) density distribution of each component for a three-component system.

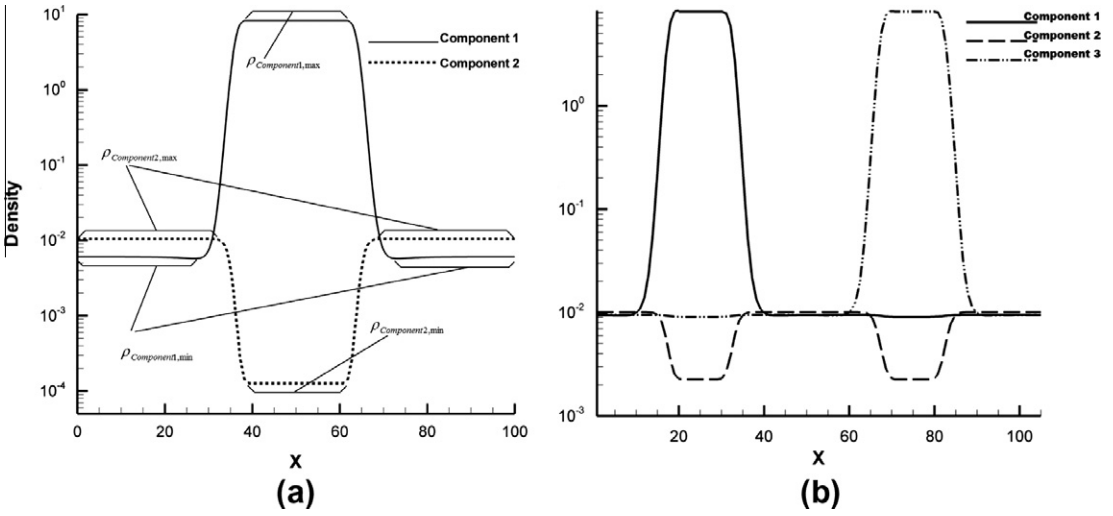

Fig. 2. Comparison of density of components along the centerline ($y = 50, 0 \leqslant x \leqslant 100$) for (a) a two-component system, and (b) a three-component system.

As we mentioned in Section 1, one of the advantages of a multi-component model is that it is possible to simulate the composition of the environment, which can be defined as $\frac{\rho_{\text{Component1,min}}}{\rho_{\text{Component1,min}}+\rho_{\text{Component2,max}}}$. For a water–air system, this composition can be considered to be the humidity. For the case shown in Figs. 1(a) and 2(a), this ratio is 2.2%, which means there are 2.2 g of water vapor in 100 g of air. This is very close to the theoretical point of a 100% relative humidity for a water vapor-air system at a temperature of 300 K (~2.2%), or a system at 50% relative humidity at a temperature of 310 K. For the three-component system, as shown in Figs. 1(b) and 2(b), the advantage of our MCMP LBE model is more obvious. It is also very easy to investigate and track the composition of each component in the atmosphere.

It should be noted here that, realistically, two unmixable components cannot occupy the same physical space at the same time. For example, in a water-oil system, water cannot flow into the space that the oil already occupies. This means that the density of water should be zero (or an extremely small value) in the area where the density of oil takes precedence. For a numerical model, it is almost impossible to have a density distribution with a zero value (or a extremely small value near zero). What can be done is to reduce the value of $\rho_{\text{Component1,min}}$ and $\rho_{\text{Component2,min}}$, or increase the ratio $\frac{\rho_{\text{Component2,max}}}{\rho_{\text{Component1,min}}}$ and $\frac{\rho_{\text{Component1,max}}}{\rho_{\text{Component2,min}}}$. As shown in Fig. 2, the ratio $\frac{\rho_{\text{Component1,max}}}{\rho_{\text{Component2,min}}}$ is on the order of 10^5, which is relatively high. However, the ratio $\frac{\rho_{\text{Component2,max}}}{\rho_{\text{Component1,min}}}$ is on the order of 10^0 to 10^2 for different cases with different system density ratios. This ratio is clearly not high enough, and therefore represents a slight deviation from the real phenomenon, especially for a high density ratio system such as that shown in Fig. 2. This issue is caused by the SCMP LBE model's limitations on the density ratio. For example, for a water–air system at a standard state (ISO: $T = 0$ °C, $P = 760$ mmHg, and $g = 9.80665$ m/s^2) there is 20 g of water vapor in 1m^3 air, so the effective density of water in this condition can be defined as 0.02 kg/m^3, while the density of water is around 1×10^3 kg/m^3. This means that, for such a system, the density ratio of a single-component $\frac{\rho_{\text{Component1,max}}}{\rho_{\text{Component1,min}}}$ should be 5×10^4, and currently no SCMP LBE model can reach such a high density ratio. Fortunately, however, the density of water vapor in the air is much high than this in many practical problems, and can even be as high as 1 kg/m^3. This is also true for other multi-component multi-phase thermal problems with other substances. Hence, our MCMP LBE model can be applied to study these systems and problems. For further extension of our MCMP LBE model, it may depend on a more powerful SCMP LBE model.

3.1.1. Ratio of maximum forces

As detailed in Section 2, the balance of the weight of the two parts $\vec{F}_{i,i}$ and $\vec{F}_{i,j}$ directly affects the density ratio of the different components. They can be adjusted through $\vec{g}_{i,i}$ and $\vec{g}_{i,j}$. The forces $\vec{F}_{i,i}$ and $\vec{F}_{i,j}$ vary in the simulation domain and reach a maximum value around the interface of the two components. In Eqs. (8a) and (8b), the gradient of the effective mass reaches its maximum value near the component/phase interface because of the significant density variation that occurs at that interface. Hence, the maximum interparticle force occurs near the interface. Fig. 3 shows the distribution of the ratio of $\vec{F}_{1,1-x}$ and $\vec{F}_{1,1,\max}$ in the test area, where $\vec{F}_{1,1-x}$ is the x-direction of the interparticle force of component 1 and $\vec{F}_{1,1-x}$ is the maximum force in the entire test region.

Hence, we set the ratio of the maximum forces $\left(\frac{\vec{F}_{1,1,\max}}{\vec{F}_{1,2,\max}}\right)$ as a key factor, and examine how this ratio affects the density ratio of the two components. The simulation is for an equilibrium droplet in a 100×100 lattice 2D square domain without body forces. Fig. 4 shows four tests in this simulation domain with the $\frac{|\vec{F}_{1,1,\max}|}{|\vec{F}_{1,2,\max}|}$ ratio set equal to 260, 75, 56, and 47. The solid line is

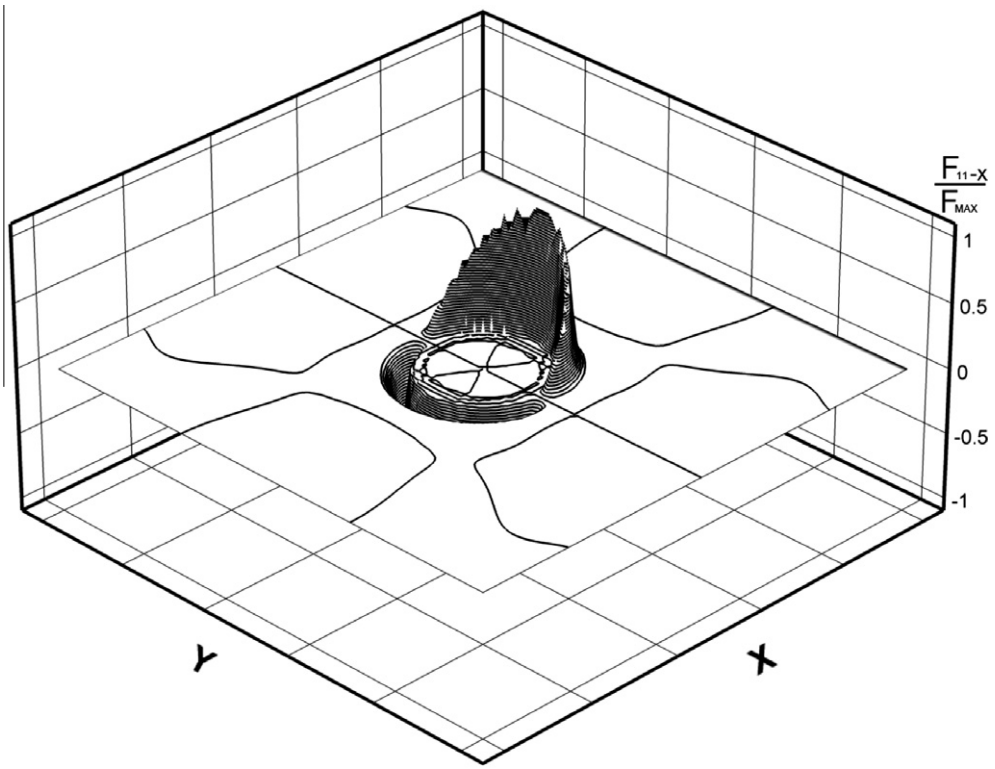

Fig. 3. Distribution of the ratio of $F_{1,1-x}$ and $F_{1,1,\max}$.

the density distribution of component 1 along the centerline ($y = 50$, $0 \leqslant x \leqslant 100$), and the dotted line is the density distribution of component 2 along the centerline. The density ratios of the two components are 278, 83, 53, and 44, respectively.

Fig. 5 shows the relationship between the density ratio and maximum force ratio. From Fig. 5, we can see that by changing the ratio of the maximum force, the density ratio can be adjusted from 1 to 1000. This is a substantial range that can cover almost all kinds of liquid–gas or liquid-liquid two component systems. One should notice that the forces $\vec{F}_{1,1}$ and $\vec{F}_{1,2}$ are in conflict when they are of the same order. Therefore, if the density ratio is around 1, the interparticle forces of the different components $\vec{F}_{1,2}$ are 1 or 2 orders of magnitude higher than the force $\vec{F}_{1,1}$ (or $\vec{F}_{1,1}$ can be directly neglected). This coincides with the actual physical phenomenon. When the density ratio of two components is very large, such as in a water–air system, the formation and position of the interface are mainly controlled by the surface tension of the water(as well as the body force and the interaction between the fluid and solid wall, if those are present). The interparticle force between the different components is very weak, especially for steady-state behavior. With a decrease in the density ratio, the interparticle force becomes more important. When the density ratio is near 1.0, like in a water-oil system, the formation and position of the interface is mainly caused by the interparticle force between the different components instead of the surface tension, body force, or other forces applied on each single component.

3.1.2. Spurious current

A spurious current around the interface is an unphysical velocity that exists in the LBE model. Much research has been focused on discovering why the spurious current exists and on reducing it. One of the explanations is that the anisotropy of the discretized momentum space causes the spurious current [41]. Hence, by modifying the LBE model, the spurious current can be decreased, but cannot be eliminated. Our MCMP LBE model performs well in reducing the spurious current to an acceptably small value. Fig. 6(a) shows the spurious current vectors in the same 2D simulation domain for a density ratio of around 1000:1, and Fig. 6(b) shows the magnitude of the spurious current.

We can see that, for a density ratio of around 1000:1, the spurious current is still under 0.032 (the main current magnitude is on the order of 10^{-13} for this equilibrium test case). This spurious current looks large compared to the surrounding velocity, but it is as good as or even better than most SCMP or MCMP LBE models. The spurious current in the most popular and widely used SCMP or MCMP LBE models may be around 0.05 to 0.1 in the same equilibrium test with a much smaller density ratio (on the order of 10^0). Furthermore, the area affected by the spurious current is very small in our MCMP LBE model. For the case with a 1000:1 density ratio, the velocity is reduced to 10^{-13} at a point $2r$ far away from the droplet center (r is the radius of the droplet), as shown in Fig. 6(b). For the cases with smaller density ratios (smaller than 300), the affected

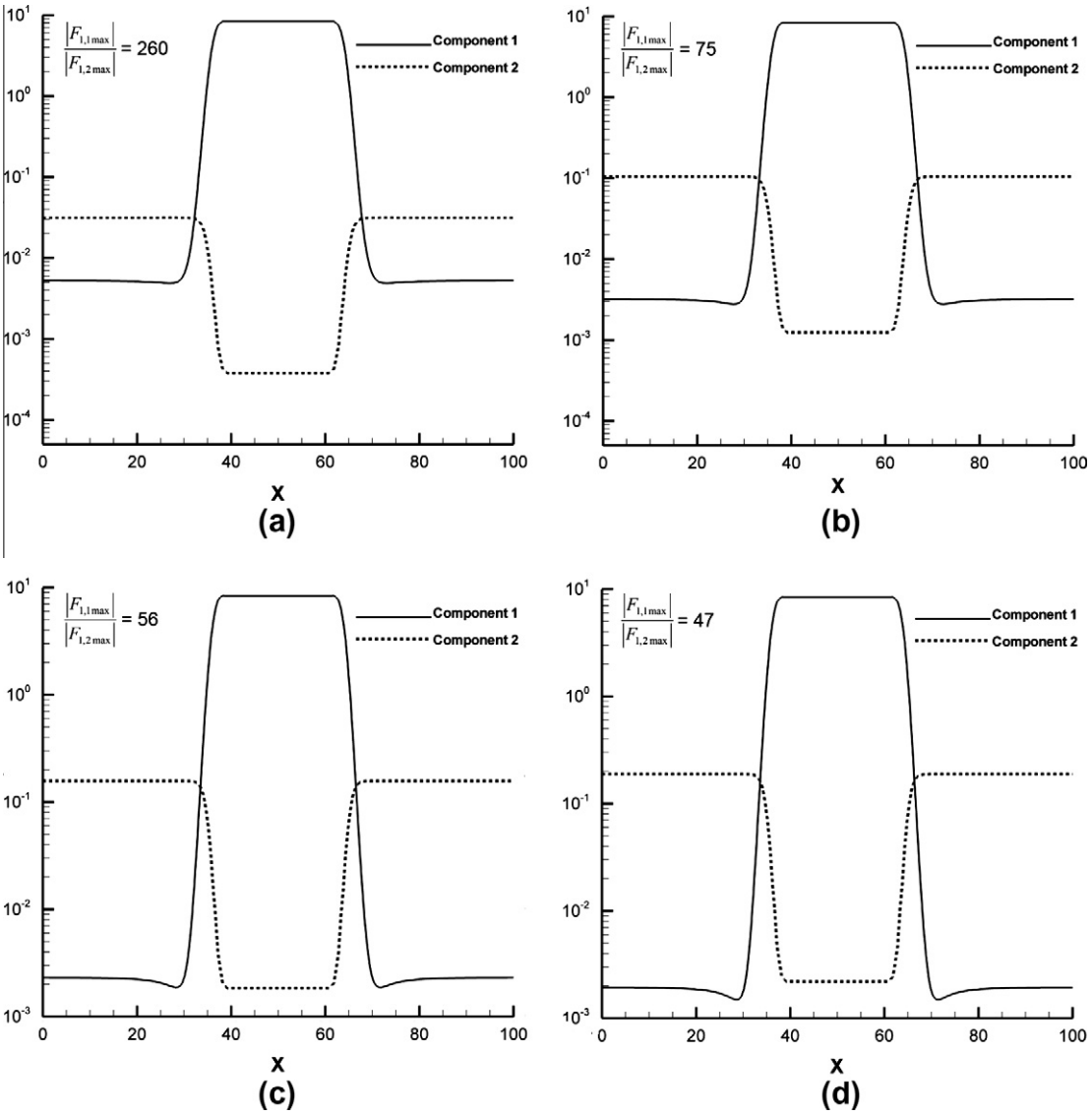

Fig. 4. Comparison of the density of the two components along the center line ($y = 50$, $0 \leqslant x \leqslant 100$) for (a) $\frac{|F_{1,1\max}|}{|F_{1,2\max}|} = 260$, (b) $\frac{|F_{1,1\max}|}{|F_{1,2\max}|} = 75$, (c) $\frac{|F_{1,1\max}|}{|F_{1,2\max}|} = 56$ and (d) $\frac{|F_{1,1\max}|}{|F_{1,2\max}|} = 47$.

area is much smaller, and the spurious current disappears at a point $1.2r \sim 1.3r$ away from the droplet center. Fig. 7 shows the relationship between the spurious current and the density ratio using our MCMP LBE model. It can be seen that the spurious current is tightly controlled for the full range of a density ratio that covers most kinds of liquid–gas and liquid-liquid systems. We also found that by using our MCMP LBE model, the spurious current is even smaller than in Yuan and Schaefer's SCMP LBE model. Fig. 7 shows the comparison between our MCMP and the SCMP LBE model. The SCMP LBE model is using P-R EOS. The magnitude of the maximum spurious current in the MCMP model is approximately half of the value in the SCMP model, especially for a density ratio over 100:1.

3.1.3. Convergence speed

Additionally, convergence is an important criteria for any numerical model. Hence, we tested the convergence speed of our MCMP LBE model for the same 2D case. Fig. 8 shows the residual with respect to the time steps. The residual here is defined as the difference between the maximum magnitude of the spurious current of two nearby time steps:

$$\text{Residual} = |\vec{u}|^{n}_{\max} - |\vec{u}|^{n-1}_{\max}. \tag{18}$$

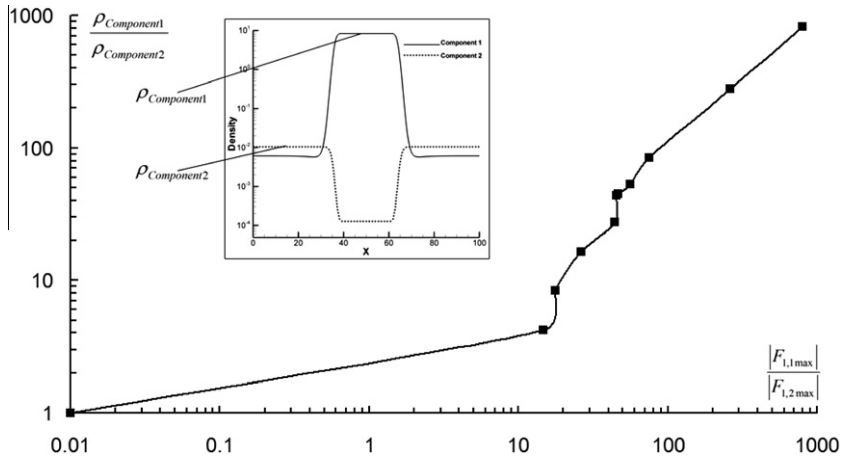

Fig. 5. Density ratio $\frac{\rho_{Component1}}{\rho_{Component2}}$ variation with the ratio of the maximum force $\frac{|F_{1,1max}|}{|F_{1,2max}|}$.

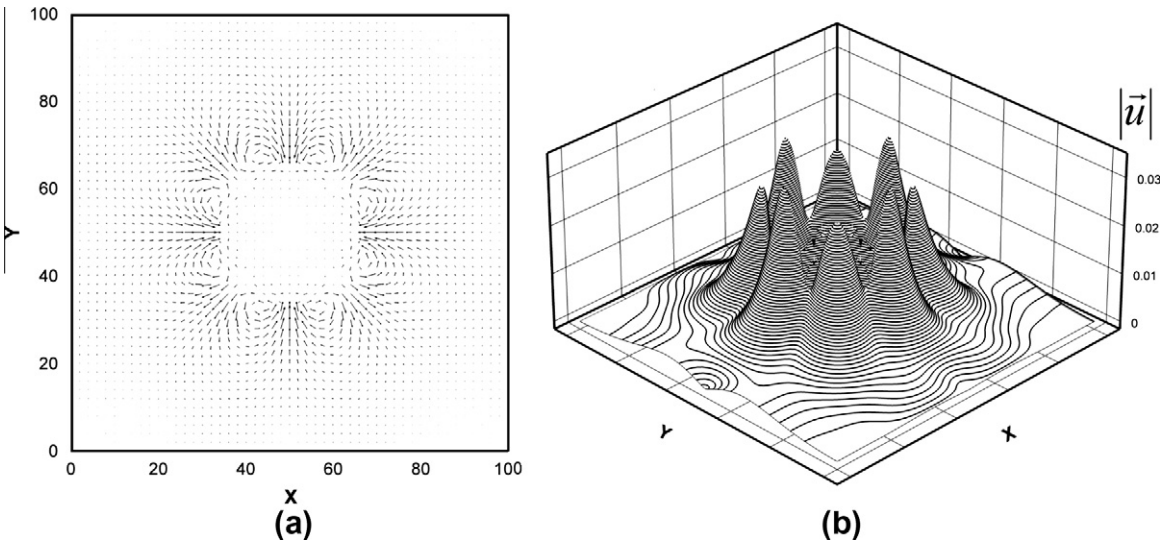

Fig. 6. (a) Vectors of the spurious current around the droplet, and (b) magnitude of the spurious current.

The case shown in Fig. 8 is again for a density ratio of around 1000:1. Before 5000 steps, the residual is already smaller than 1.0×10^{-16}, and near 30,000 steps, the residual reaches 1.0×10^{-16}. For those cases with a smaller density ratio, the model converges faster.

3.2. Simulation of an equilibrium droplet affected by a body force and external forces

One of the strengths of the LBE model, besides its ability to simulate MCMP flow, is its flexibility for applying body and external forces on a flow. Hence, this second example is a refinement of the first one. The boundary conditions and the number of grids are the same as in Section 3.1, but we also add gravity along the negative y-direction in the simulation domain, and the interaction between the fluids and the solid boundary is considered. Eqs. (9) and (10) are used to calculate these two forces. The value of G_w controls the force between the fluid nodes and solid nodes. A positive G_w represents a repulsive force, which means that the solid wall repels the fluid and acts as a hydrophobic surface. A negative G_w represents an attractive force, or hydrophilic surface. The contact angle can clearly reflect the property of the interaction between the solid surface (smaller than 90° for a hydrophilic surface, greater than 90° for a hydrophobic surface). Fig. 9 shows the position of the interface of the two components. Fig. 9(a) is a droplet on a hydrophilic surface whose contact angle (θ) is about 45° and Fig. 9(b) shows a droplet on a hydrophobic surface with a 115° contact angle. We can see that our MCMP LBE model inherits the original LBE model's flexibility in dealing with the external forces and body force. It should be noted that the contact angle is controlled by both of the fluids near the solid–fluid interface. For a high density ratio, these co-effects are not strong, and the

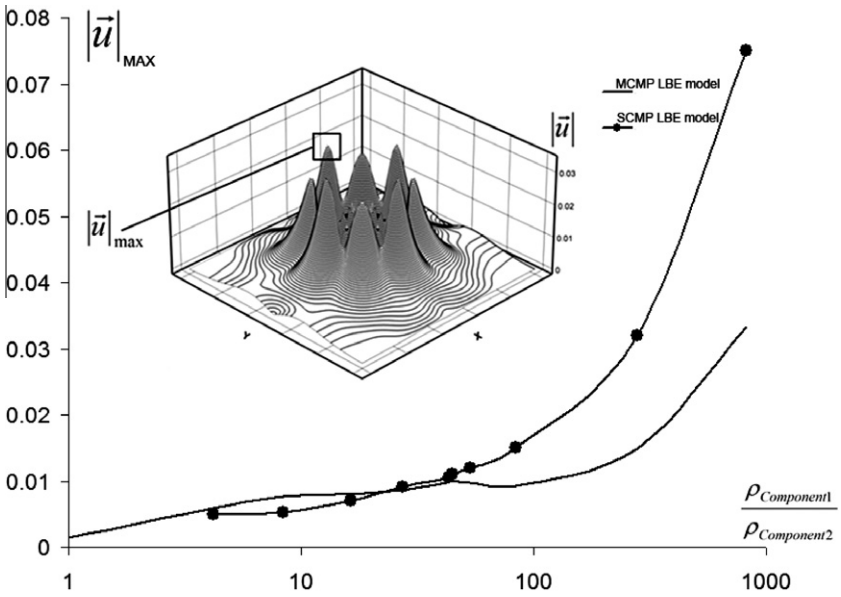

Fig. 7. Comparison of the maximum magnitude of the spurious currents between our MCMP and a SCMP LBE model varying with the density ratio.

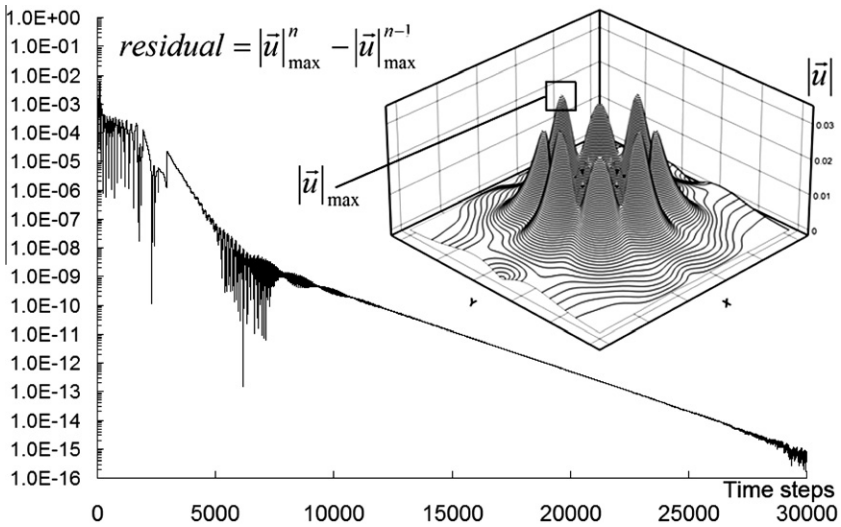

Fig. 8. The residual change with time steps.

contact angle is mainly controlled by the fluid with the high density. For a small density ratio, these co-effects become strong.

3.3. Simulation of a droplet in a flow

This third example is a further refinement of the second one. Based on Section 3.2, we add a pressure drop along the positive x direction, where $\frac{dP}{dx}$ equals 2×10^{-5} in lattice units. The system density ratio is about 300:1. Fig. 10 shows the position of the interface of the two components and the velocity vector in the simulation domain. The main current magnitude is on the order of 10^{-1}, and the spurious current is too small to be observed compared to the main current. As expected for a hydrophilic surface, in Fig. 10(a), the two contact angles θ_1 and θ_2 are different. This difference reflects the different attractive forces at the two contact points, and represents the contact angle hysteresis phenomena. In Fig. 10(b), the two contact angles θ_1 and θ_2 are almost the same, which means that the repulsive forces at the two contact points are almost the same, and the drag force is very small. This coincides with the real physical phenomenon. The drag force on a hydrophobic surface is very small, and, for the ideal hydrophobic surface, the drag force should be zero.

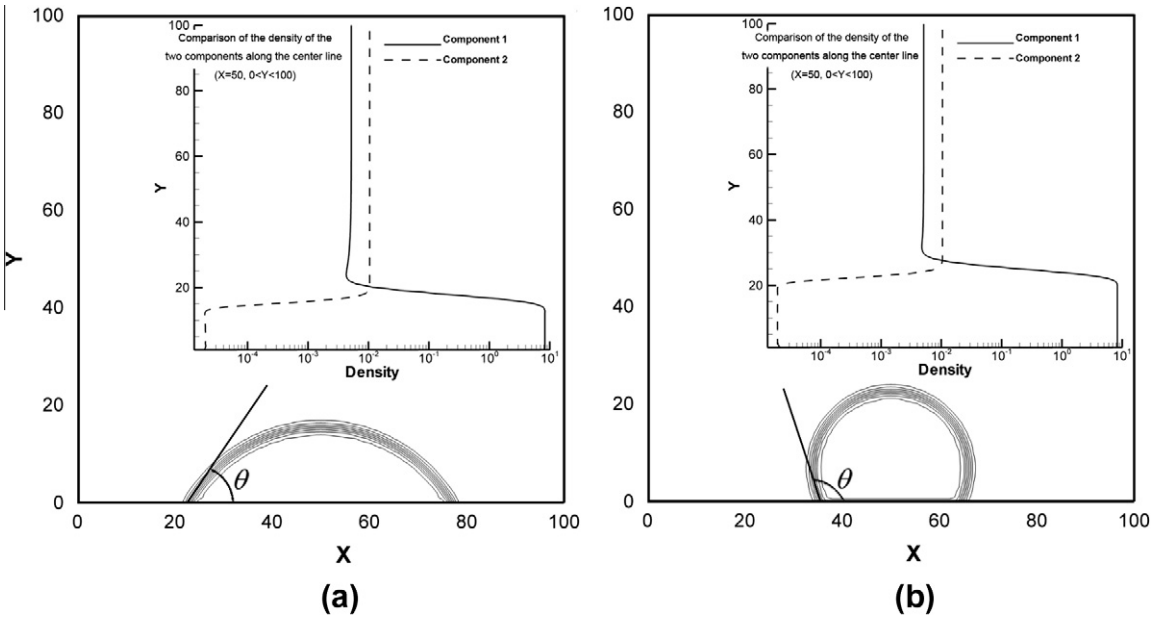

Fig. 9. Position of the interface of the two components on a hydrophilic (a) and hydrophobic (b) surface, and comparison of the density of the two components along the centerline ($x = 50$, $0 \leqslant y \leqslant 100$).

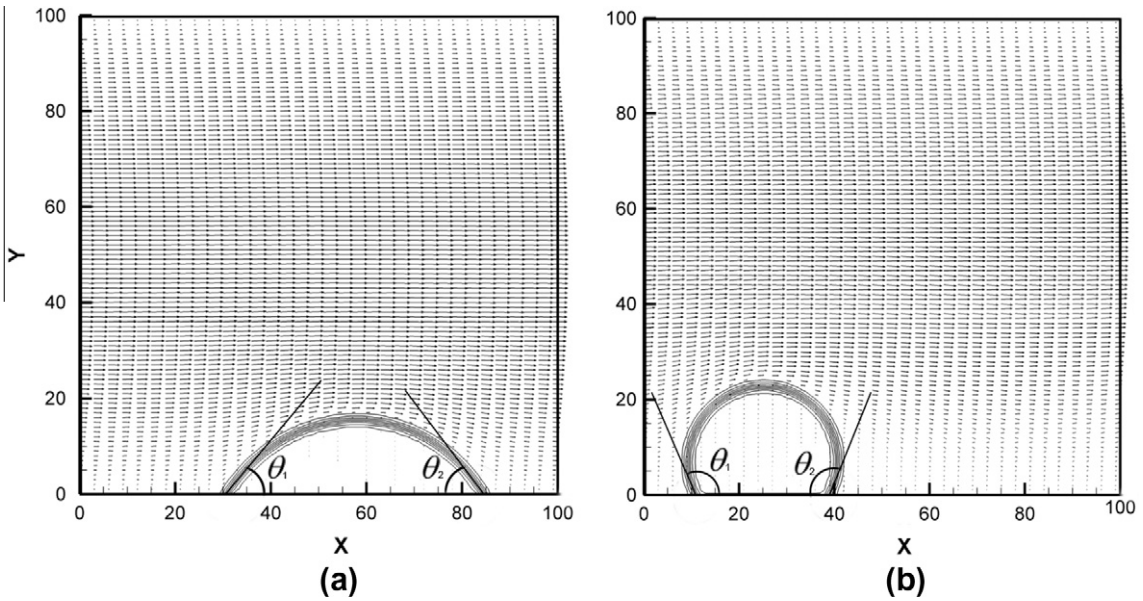

Fig. 10. Position of the interface of the two components and the velocity vectors for (a) a hydrophilic surface, and (b) a hydrophobic surface.

4. Conclusions and discussion

The theoretical basis presented in Section 2 and the simulation results detailed in Section 3 show that applying a more realistic EOS for at least one component (particularly the liquid component) instead of using the SC EOS is a precondition for increasing the density ratio of a MCMP flow system. Additionally, the balance between the forces $\vec{F}_{i,j}$ and $\vec{F}_{i,j}$ play an important role in adjusting a MCMP system's density ratio. In previous MCMP LBE models, the interaction between molecules of the same component ($\vec{F}_{i,j}$) had not received enough attention. We found that by increasing the fraction of $\vec{F}_{i,j}$ in the sum of $\vec{F}_{i,j}$ and $\vec{F}_{i,j}$, the density ratio can increase substantially. One advantage of our MCMP model is that it makes it possible to simulate and investigate the composition of the gas. The model also offers a base for simulation of heat transfer phenomena for

high density ratio systems. All of the results in Section 3 are for a relatively simple case in order to clearly demonstrate our MCMP LBE model's performance. For future research, other more realistic systems or problems should be tested, such as those with more complicated solid boundaries, a more sophisticated interface, dynamic problems, and moving boundary conditions.

References

[1] F.H. Harlow, J.E. Welch, Numerical calculation of time-dependent viscous incompressible flow, Phys. Fluids 8 (1965) 2182–2189.
[2] B.J. Daly, Numerical study of the effect of surface tension on interface instability, Phys. Fluids 12 (1969) 1340–1354.
[3] C.W. Hirt, B.D. Nichols, Volume of fluid (VOF) method for the dynamics of free boundaries, J. Comput. Phys. 39 (1981) 201–225.
[4] J.A. Sethian, Level Set Methods: Evolving Interfaces in Geometry, Fluid Mechanics, Computer Vision, and Materials Science, Cambridge University Press, 1996.
[5] S.O. Unverdi, G. Tryggvason, A front-tracking method for viscous, incompressible, multi-fluid flows, J. Comput. Phys 100 (1992) 25–37.
[6] A.R. Wadhwa, V. Magi, J. Abraham, Numerical studies of droplet interactions, in: Proceedings of International Conference on Liquid Atomization and Spray Systems, Sorrento, Italy, July 2003.
[7] G. Tryggvason, B. Bunner, A. Esmaeeli, D. Juric, N. Al-Rawahi, W. Tauber, J. Han, S. Nas, Y.J. Jan, A front-tracking method for the computations of multiphase flow, J. Comput. Phys. 162 (2001) 708–759.
[8] S.G. Yoon, A Fully Nonlinear Model for Atomization of High-Speed Jets, Ph.D. thesis, Purdue University, 2002.
[9] T. Inamuro, M. Yoshino, H. Inoue, R. Mizuno, F. Ogino, A lattice Boltzmann method for a binary miscible fluid mixture and its application to a heat-transfer problem, J. Comput. Phys. 179 (2002) 201–215.
[10] M.C. Sukop, D.T. Thorne, Lattice Boltzmann modeling: An Introduction for Geoscientists and Engineers, first ed., Springer, 2005.
[11] L.-S. Luo, The lattice-gas and lattice Boltzmann method: past, present, and future, Proceedings of the International Conference on Applied Computational Fluid Dynamics, Beijing, China, 2000. pp. 52–83.
[12] A.K. Gunstensen, D.H. Rothman, S. Zaleski, G. Zanetti, Lattice Boltzmann model of immiscible fluids, Phys. Rev. A 43 (1991) 4320–4327.
[13] D.H. Rothman, J.M. Keller, Immiscible cellular-automaton fluids, J. Stat. Phys. 52 (3) (1988) 1119–1127.
[14] X. Shan, H. Chen, Lattice Boltzmann model for simulation flows with multiple phases and components, Phys. Rev. E 47 (1993) 1815–1819.
[15] X. Shan, H. Chen, Simulation of nonideal gases and liquid–gas phase transitions by the lattice Boltzmann equation, Phys. Rev. E 49 (1994) 2941–2948.
[16] X. Shan, G.D. Doolen, Multicomponent lattice-Boltzmann model with interparticle interaction, J. Stat. Phys. 81 (1995) 379–393.
[17] X. Shan, D. Doolen, Diffusion in a multicomponent lattice Boltzmann equation model, Phys. Rev. E 54 (1996) 3614–3620.
[18] S. Hou, X. Shan, Q. Zou, G.D. Doolen, W.E. Soll, Evaluation of two lattice Boltzmann models for multiphase flows, J. Comput. Phys. 138 (2) (1997) 695–713.
[19] S. Leclaire, M. Reggio, J.-Y. Trépanier, Numerical evaluation of two recoloring operators for an immiscible two-phase flow lattice Boltzmann model, Appl. Math. Model. 36 (5) (2012) 2237–2252.
[20] M. Latva-Kokko, D.H. Rothman, Diffusion properties of gradient-based lattice Boltzmann models of immiscible fluids, Phys. Rev. E 71 (2005) 056702.
[21] T. Reis, T.N. Phillips, Lattice Boltzmann model for simulating immiscible two-phase flows, J. Phys. A: Math. Theor. 40 (14) (2007) 4033–4053.
[22] M. Swift, W. Osborn, J. Yeomans, Lattice Boltzmann simulation of nonideal fluids, Phys. Rev. Lett. 75 (1995) 830–833.
[23] M. Swift, S. Orlandini, W. Osborn, J. Yeomans, Lattice Boltzmann simulations of liquid–gas and binary-fluid systems, Phys. Rev. E 54 (1996) 5041–5052.
[24] R. Nourgaliev, T. Dinh, T. Theofanous, D. Joesph, The lattice Boltzmann equation method: theoretical interpretation, numerics and implications, Int. J. Multiphase Flow 29 (2003) 117–169.
[25] X. He, S. Chen, R. Zhang, A lattice Boltzmann scheme for incompressible multiphase flow and its application in simulation of Rayleigh–Taylor instability, J. Comput. Phys. 152 (1999) 642–663.
[26] X. He, R. Zhang, S. Chen, G.D. Doolen, On the three-dimensional Rayleigh-Taylor instability, Phys. Fluids 11 (5) (1999) 1143–1152.
[27] Q. Kang, D. Zhang, S. Chen, Displacement of a three-dimensional immiscible droplet in a duct, J. Fluid Mech. 545 (2005) 41–66.
[28] H.W. Zheng, C. Shu, Y.T. Chew, A lattice Boltzmann model for multiphase flows with large density ratio, J. Comput. Phys. 218 (1) (2006) 353–371.
[29] T. Lee, C.-L. Lin, A stable discretization of the lattice Boltzmann equation for simulation of incompressible two-phase flows at high density ratio, J. Comput. Phys. 206 (1) (2005) 16–47.
[30] T. Inamuro, T. Ogata, S. Tajima, N. Konishi, A lattice Boltzmann method for incompressible two-phase flows with large density differences, J. Comput. Phys. 198 (2) (2004) 628–644.
[31] J. Kim, Phase field computations for ternary fluid flows, Comput. Methods Appl. Mech. Eng. 196 (2007) 4779–4788.
[32] P.L. Bhatnagar, E.P. Gross, M. Krook, A model for collision processes in gases. I. Small amplitude processes in charged and neutral one-component system, Phys. Rev. 94 (1954) 511–525.
[33] P. Yuan, Thermal Lattice Boltzmann Two-phase Flow Model for Fluid Dynamics, Ph.D. thesis, University of Pittsburgh, 2005.
[34] X. He, L. Luo, A priori derivation of the lattice Boltzmann equation, Phys. Rev. E 55 (1997) R6333–R6336.
[35] D. Kandhai, A. Koponen, A. Hoekstra, M. Kataja, J. Timonen, P.M.A. Sloot, Implementation aspects of 3D lattice-BGK: boundaries, accuracy, and a new fast relaxation method, J. Comput. Phys. 150 (1999) 482–501.
[36] P.G. de Gennes, Wetting: statics and dynamics, Rev. Mod. Phys. 57 (1985) 827–863.
[37] R. Benzi, S. Succi, M. Vergassola, The lattice Boltzmann equation: theory and applications, Phys. Rep. 222 (1992) 145–197.
[38] R. Zhang, Lattice Boltzmann Approach for Immiscible Multiphase Flow, Ph.D. thesis, Department of Mechanical Engineering, University of Delaware, 2000.
[39] P. Yuan, L. Schaefer, Equations of state in a lattice Boltzmann model, Phys. Fluids, 18, 2006.
[40] Y.S. Wei, R.J. Sadus, Equations of state for the calculation of fluid-phase equilibria, AIChE J. 46 (1) (2000) 169–196.
[41] M. Sbragaglia, R. Benzi, L. Biferale, S. Succi, K. Sugiyama, F. Toschi, Generalized lattice Boltzmann method with multirange pseudopotential, Phys. Rev. E 75 (2007) 026702.